

**NON-DESTRUCTIVE TEST FOR QUALITY CONTROL IN LABORATORY-SCALE
FABRICATION OF LAMINATED COMPOSITES USING PROGRAMMABLE PORTABLE
ULTRASONIC**

*Yusuf Giri Wijaya^{a, b}, Suprijanto^{c, *}, Damar Rastri Adhika^{d, e}, Rhakamerta Hijazi^{a, f}, Abian Nurrohmadi^b*

^a Magister Program of Instrumentation and Control, Faculty of Industrial Technology, Institut Teknologi Bandung, Bandung, Indonesia

^b Research Center for Aeronautics Technology, National Research and Innovation Agency, Bogor, Indonesia

^c Instrumentation, Control and Automation Research Group, Faculty of Industrial Technology, Institut Teknologi Bandung, Bandung, Indonesia

^d Nano and Quantum Technology Research Group, Engineering Physics, Faculty of Industrial Technology, Institut Teknologi Bandung, Indonesia

^e Research Center for Nanosciences and Nanotechnology, Institut Teknologi Bandung, Indonesia

^f Research Center for Nuclear Beam Analysis Technology, National Research and Innovation Agency, Tangerang, Indonesia

* Corresponding author. E-mail address: supri89@itb.ac.id

NON-DESTRUCTIVE TEST FOR QUALITY CONTROL IN LABORATORY-SCALE FABRICATION OF LAMINATED COMPOSITES USING PROGRAMMABLE PORTABLE ULTRASONIC

Abstract

Laminated composites are the most frequently used component materials in manufacturing unmanned aerial vehicles (UAVs) in research centers or start-up industries. On a laboratory scale, laminated composites are fabricated by relying on technicians' skills due to the involvement of manual processes. Non-destructive testing (NDT) is needed to guarantee the structural integrity of the final product of laminated composites. The work proposes a programmable portable ultrasonic for non-destructive testing (NDT) to detect a potential defect due to foreign object contamination of fabrication layers of laminate composite. The proposed programmable NDT system is built using open-board devices; therefore, it could be developed cost-effectively compared to a commercial NDT system. The proposed NDT can measure and analyze a pattern of A-scan signal as a function of foreign object contamination material. Based on a C-scan image, the proposed NDT system could also be programmed to detect the size area of potential defects due to foreign object contamination. Two types of specimens, carbon fiber-reinforced polymer (CFRP) and glass fiber-reinforced polymer (GFRP), were tested to evaluate the performance of the developed NDT system. Testing aims to identify artificial defects intentionally placed within these specimens. The proposed portable ultrasonic NDT effectively detects CFRP and GFRP defects on A-mode and C-scan images. Therefore, the proposed portable ultrasonic NDT is an affordable system that can be developed in a laboratory workshop for quality control in laboratory-scale fabrication of laminated composites.

Keywords: *Laminated composite, laboratory-scale fabrication, quality control, portable ultrasonic NDT, A-scan, C-scan*

1. INTRODUCTION

Composite materials made from fibers and polymer matrices are widely used in the aerospace, automotive, and marine industries. Their main benefits include lightweight yet durable construction, the ability to reduce vibrations, good corrosion resistance, effective thermal insulation properties, and the ability to form structures with complex shapes [1]. Laminated composites are the most commonly used composite material in producing unmanned aerial vehicles (UAVs) in research centers and small industries. Laminated composites are made by assembling several layers of fibers and combining them with resin. The mechanical properties of laminated composites can be specifically designed according to the requirements of the UAV components. Selecting fiber types and resin composition is crucial to achieving the desired properties of laminated composites. Commonly used fibers in producing laminated composites include E-glass, carbon, and Kevlar [2], while frequently used resins are epoxy, polyester, and vinyl ester [3].

Research centers and small industries usually manufacture laminated composites on a laboratory scale to produce UAV prototypes due to cost-effective methods. The methods used to produce laminated composites include hand lay-up, vacuum bagging, vacuum-assisted resin infusion (VARI), and prepreg [4]. Hand lay-up and vacuum bagging is a fabricated laminated composite that offers minimum investment in equipment.

However, using both methods, the quality control of laminate, fiber volume fraction, and consistency of the material's strength is difficult to keep consistent for each batch fabrication. The prepreg method is pre-impregnated with fully curable composite fibers, and a mixed resin system is used during manufacture. The preps serve as the basic building block to fabricate high-performance composite structures. However, the Prepreg method is relatively costly and requires various types of equipment suitable for fabrication on an industry scale [5]. A moderate solution that balances the production of composite materials for UAV structures is using the VARI method due to the excellent mid-range composite fabrication process that offers reasonable investment in equipment for fabrication at a laboratory scale and quality of strength and homogeneity [6].

VARI method is a fabricated laminated composite that uses negative pressure to infiltrate a resin into a laminated fiber reinforcement. The fibrous component is placed dry into the mold, and the vacuum is applied before the resin is added. The fabrication of laminated composites using VARI methods has the potential to introduce several defect conditions that may reduce the strength of a final product. The defect of laminated composites may occur due to voids, porosity, delamination, misaligned fibers, and foreign object contamination [7]. NDT must be conducted after fabrication to guarantee the structural integrity and safety of the final product of laminated composites. Several NDT methods exist for composite materials, such as X-ray radiography, Ultrasonic Testing, Infrared Thermography, and Acoustic Emission [8]. However, ultrasonic testing has been one of the most extensively used NDT technologies due to its safety, portability, and relative ease of use compared to other NDT methods [9].

Ultrasonic NDT aims to obtain ultrasonic wave signal patterns reflected from laminated composite samples and process them to distinguish between defect and non-defect signals. The result of this processing is known as the A-scan signal. An A-scan signal is a one-dimensional representation of the amplitude of the reflected ultrasonic wave. It can be used to identify defects at a single testing point. Furthermore, to evaluate defects for an entire surface of the specimen, A-scan signals from multiple scanning points are collected and processed into a C-scan image. A C-scan image is a two-dimensional representation that provides visual information about the location and size of defects across the entire surface of the specimen. The results of the C-scan image could be used to predict the size and distribution of defects within the material more accurately and effectively.

Many researchers have reported the advantageous application of Ultrasonic NDT for testing the structural integrity of laminate composite [10]. However, most researchers use commercial main boards of ultrasonic NDT systems, particularly electronic boards for pulser, receivers, high-speed ADCs, and software for signal processing [11]. For small research laboratories that develop small-range and mid-range UAVs, an Ultrasonic NDT system with specifications such as a programmable system to easy modification follow target inspection, portable, good performance, and relatively low-cost development are required. Portability guarantees the equipment's ease of transportation and usability in various locations, particularly for field testing. Furthermore, the A-scan signal of the Ultrasonic NDT system can be configured as a C-scan ultrasonic NDT to produce a 2D mapping of the internal material of the laminated composite.

In this paper, we propose developing a programmable portable ultrasonic NDT system to support quality control in the laboratory-scale fabrication of laminated composite. An open primary board device of an ultrasonic NDT system reported on [12], [13] was chosen. These open-board devices were also integrated with a water immersion tank with an axis scanning arm to reconstruct C-scan ultrasound images. The proposed programmable portable ultrasonic NDT system was used to evaluate the system's ability to detect a potential defect due to a foreign object contamination of fabrication layers of laminate composite. The pattern of the A-scan signal as a function material type of foreign object contamination was further processed and analyzed using our proposed ultrasonic NDT system. Furthermore, the size of potential defects due to foreign object contamination was imaged using a C-scan image.

2. MATERIAL AND METHOD

2.1. SPECIMENS FABRICATION

The common types of laminated composite materials used in UAV structures are carbon fiber-reinforced polymer (CFRP) and glass fiber-reinforced polymer (GFRP) [14], [15], [16]. The primary difference between these two laminated composites lies in the fibers used. CFRP consists of multiple layers of carbon fibers combined with resin, while GFRP comprises several layers of E-glass fibers combined with resin. In UAV structures, CFRP is often used for manufacturing landing gears [17]. Carbon fibers are selected based on the strength and stiffness required to withstand significant loads and stresses during landing. Carbon fibers offer substantial strength and lighter weight than metals or E-glass, making them an ideal choice for this application.

Conversely, GFRP is widely used to make skins on the fuselage and wings. The selection of GFRP is based on several factors, including the flexibility and cost-effectiveness of E-glass compared to carbon fibers. Additionally, E-glass possesses excellent dielectric properties, which are crucial for fuselages that may interact with various communication and radar systems [18]. Examples of the use of CFRP and GFRP laminated composites in UAVs can be seen in Figure 1.

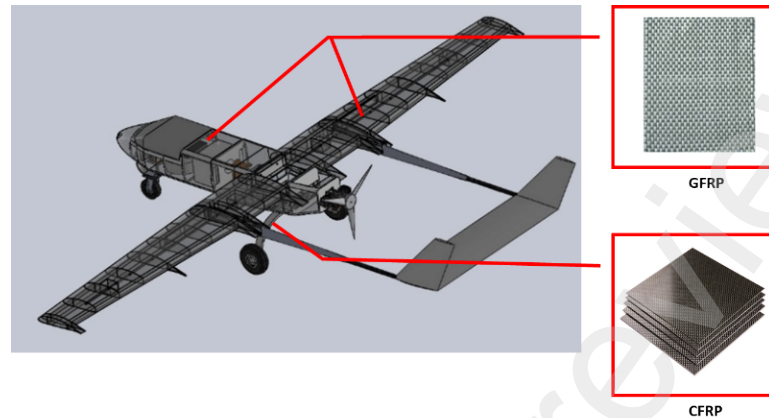


Figure 1. Examples of using laminated composite materials in UAVs [19]

In this study, two types of specimens were created to test the performance of the developed ultrasonic NDT system and to understand the differing characteristics related to ultrasonic wave phenomena in these specimens. Type I specimen is a CFRP laminated composite of carbon fibers combined with resin. Type II specimen is a GFRP laminated composite of E-glass fibers combined with resin. The resin used for both specimens combines 100% vinyl ester, 1% Percumyl H (catalyst), and 0.3% cobalt (hardener). Both specimens were designed to mimic the skin of UAV structures, forming thin sheets. The specimen sizes were reduced to 200 mm x 200 mm for easy handling and laboratory testing and to save materials and production time. Each specimen was made from ten fiber layers. After fabrication, the CFRP specimen had a thickness of 2.3 mm and a weight of 136 grams, while the GFRP specimen had a thickness of 2.3 mm and a weight of 168 grams. Based on these weights and volumes, the density values obtained were 1478 kg/m³ for the CFRP specimen and 1826 kg/m³ for the GFRP specimen.

Both specimens were created using the VARI technique. The fabrication began with preparing a clean mold coated with a release agent to facilitate the removal of the composite. Given that the specimens were thin plates, the mold was made from glass sheets placed on a table, chosen for its smooth and flat surface. The mold edges were sealed with double-sided tape to prevent resin overflow and to secure the vacuum plastic. Ten layers of carbon fiber or E-glass fiber were cut to the desired size and placed in the mold, and a resin distribution mesh was used to ensure even resin spread.

This entire assembly was then covered with vacuum plastic attached to the tape-sealed mold edges, creating a vacuum-capable mold. A vacuum pump created a negative pressure within the mold, drawing the resin through tubing to fully infiltrate the fibers without air bubbles. Once the resin was evenly distributed, the vacuum pump was turned off, and the composite was left to cure at room temperature for 24 hours to ensure thorough drying. Figure 2 illustrates the specimen fabrication process using the VARI method.

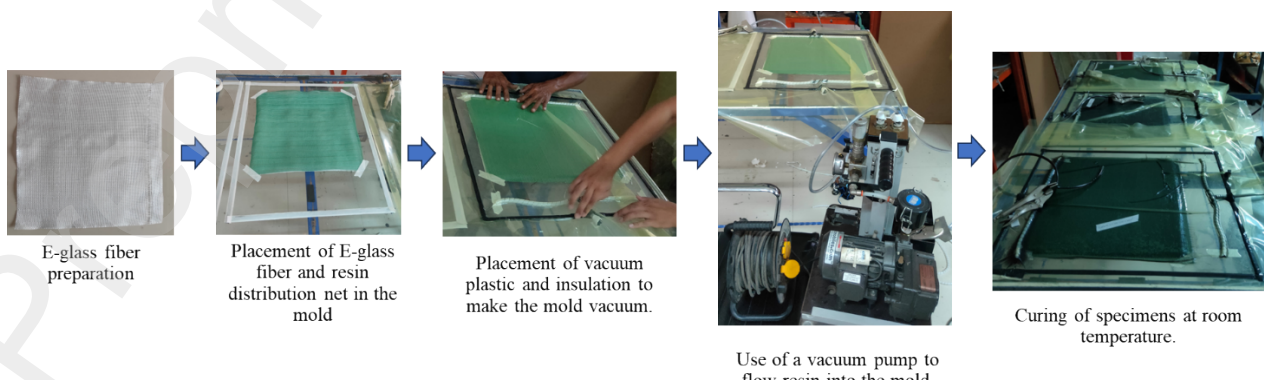


Figure 2. The specimen fabrication process using the VARI method on a laboratory scale

Although the resin infusion into the mold utilized a vacuum pump to reduce the potential for uneven resin distribution, much of the process remained manual. The manual handling in specimen fabrication heavily relies on the technician's skill, leading to the possibility of defects during production. These defects may arise from contaminants entering the resin, air bubbles within the resin, uneven resin coating on the fibers, and damage to the fibers.

In this study, intentional defects were introduced into the specimens to simulate the presence of foreign materials. This simulation aimed to evaluate the capability of the developed ultrasonic testing system in detecting and identifying these defects. Introducing deliberate defects makes testing more realistic and relevant to practical industrial applications.

The artificial defects were made from thin Teflon material shaped into circles with a radius of 15 mm. Previous research has commonly used Teflon to simulate defects [20]. Each specimen contained two artificial defects placed at different locations and depths. Defect location 1 was placed between the third and fourth fiber layers, while defect location 2 was between the seventh and eighth fiber layers. The variation in defect location and depth was intended to examine the impact of depth on the defect identification process. Figure 3 illustrates the design of defect simulation within the specimens, with the thickness of each layer being 0.2 mm.

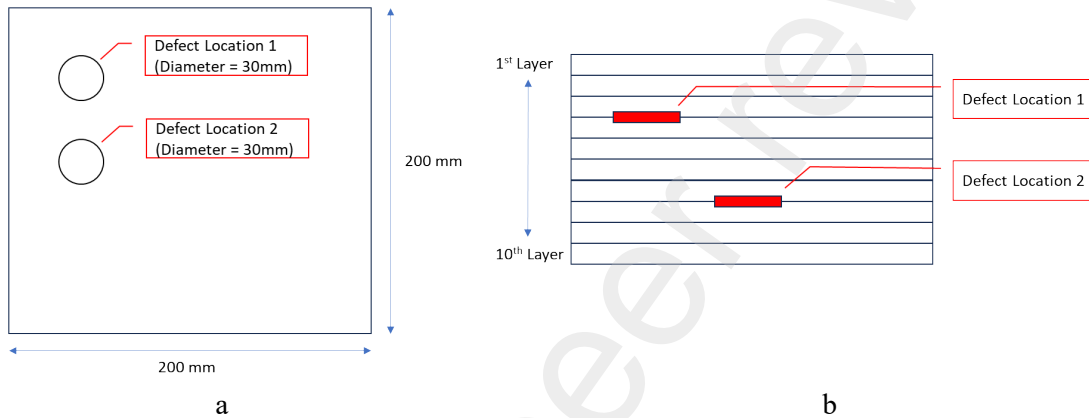


Figure 3. Shape and location of artificial defects in specimens (a) top view, (b) side view

For benchmarking purposes in testing with the developed ultrasonic system, defects in the specimens were photographed using a digital camera. The defect photography process involved placing LED lights beneath the specimen to enhance the contrast of the defects. This process was only effective for GFRP specimens due to their transparency, while defects in CFRP specimens were not visible because of their opaque and dark characteristics. Nonetheless, since the shape and size of the defects were identical, the photographs of the GFRP specimens could serve as a benchmark for testing both types of specimens. Figure 4 shows the photographs of the defects embedded within the GFRP specimens.

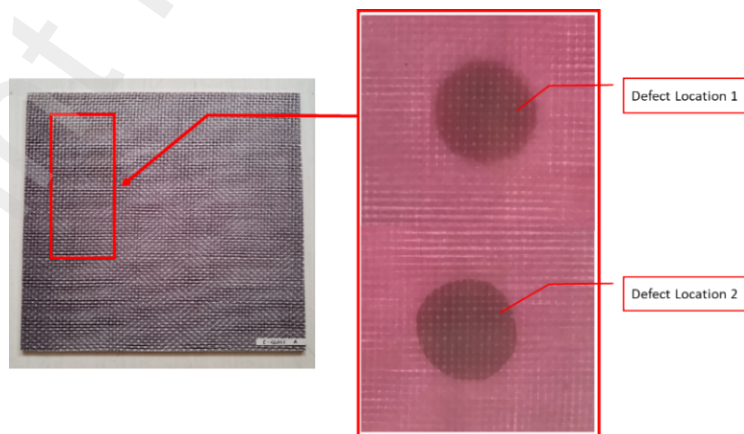


Figure 4. Defect images of GFRP specimens that were photographed using the digital camera by placing a light source beneath the specimen. The area size of artificial defects in specimens that are shown in the image used as benchmarking the results of the proposed ultrasonic NDT system

2.2. PROGRAMMABLE PORTABLE ULTRASONIC NDT SYSTEM

The primary hardware device of digital ultrasonic NDT consists of an ultrasound transducer, a pulser electronic device used to transmit electrical pulse signal to an ultrasonic transducer, a receiver, and high-speed analog to digital converter (ADC) devices that converts the ultrasonic pulse back into a digital electrical signal.

The ultrasonic transducer generates pulses that travel through the water and into the specimen. When these pulses encounter boundaries, such as the specimen's front wall, back wall, or defects, they are reflected to the transducer, creating echoes. The echo reflected from the specimen's front wall is known as the front wall echo (FWE), the echo from the back wall is known as the back wall echo (BWE), and echoes from defects are referred to as defect echoes.

With this primary configuration, the system can be utilized for ultrasonic testing on specimens using a point-by-point testing method. Each point on the specimen is individually tested to detect the presence of defects or material inconsistencies. The results of the point-by-point ultrasonic testing can be represented in the form of an A-scan. The A-scan provides a detailed depiction of defects within the specimen at each testing point and offers insights into the characteristics of ultrasonic wave propagation.

For the C-scan image, the minimizing system of additional hardware is a water immersion tank with an axes scanning arm used to move the ultrasound transducer on each point measurement. Based on the A-scan signal, a scheme of signal processing and a C-scan image reconstruction algorithm were required [21]. The results of the Ultrasonic C-scan represent the 2D image in which the contrast or color gradient indicates the condition of the specimen's surface or internal structure, highlighting the presence of defects or anomalies. Each pixel in the image corresponds to a specific location and condition on the material's surface.

In ultrasonic C-scan testing, the specimen is placed in a water-filled tank. The water acts as a couplant to ensure no air gap between the transducer and the specimen, facilitating consistent and efficient transmission of ultrasonic waves. The transducer, which emits and receives ultrasonic waves, is moved over the specimen in a precise, controlled pattern using an automated scanning system. An automated system ensures accurate transducer positioning and movement, reducing testing time compared to manual methods. This system also allows repeatable scans over the same area, ensuring consistent results.

The development of a portable ultrasonic NDT system in this research consists of several key components: an ultrasonic transducer, a scanning system integrated with a water tank, a pulser and ultrasonic measurement system, and a computer. The system architecture of the developed ultrasonic NDT system is depicted in Figure 5.

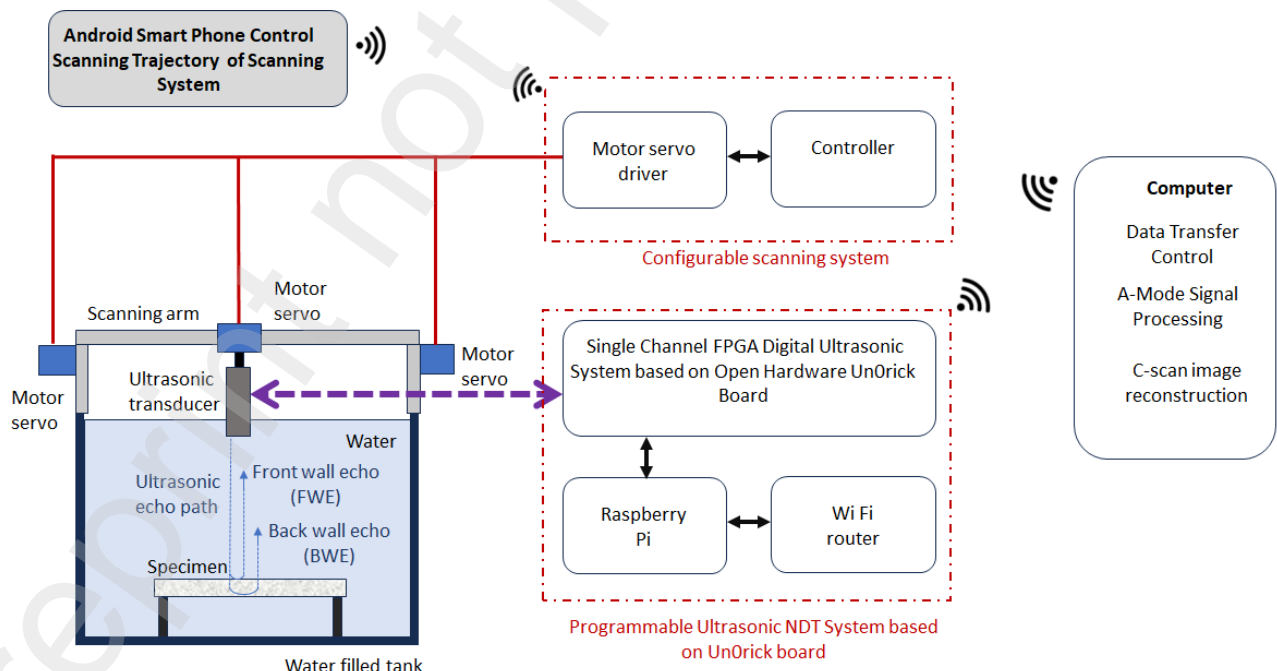


Figure 5. The system architecture of the developed ultrasonic NDT system

The primary open-board devices of the programmable ultrasonic NDT system are based on the Unorick board Single Channel FPGA. Its board functions as a pulser, a receiver, and a high-speed ADC [22]. Wireless data communication between the open-board device and the computer could be configured using a Raspberry Pi as an interface board. The Raspberry Pi configures the Unorick board parameters and temporarily stores the measurement results. The setup step is performed to configure the pulse width, number of pulses, and duration of the data acquisition process. The firmware could be set up to incorporate these parameters. The firmware is available for access and download on the Unorick website [25]. In addition, the computer is used to process the measurement data further, allowing for further data processing and visualization techniques for interpreting ultrasonic NDT tests.

For the C-scan image, an axes scanning arm was adapted from open CNC machines designed to move the ultrasound transducer on each point measurement [26]. Some modifications are applied for ultrasonic NDT scanning systems. This scanning system employs the ESP32 as the central controller. In addition to controlling the movement of the stepper motors, the ESP32 is also used for the communication system, enabling connection through a graphical user interface (GUI) based on applications that run on Android [27]. A trajectory movement of the ultrasonic transducer on the scanning system could be easily set up using Web-based GUI on the smartphone. Figure 6 presents the design of the configurable scanning system.

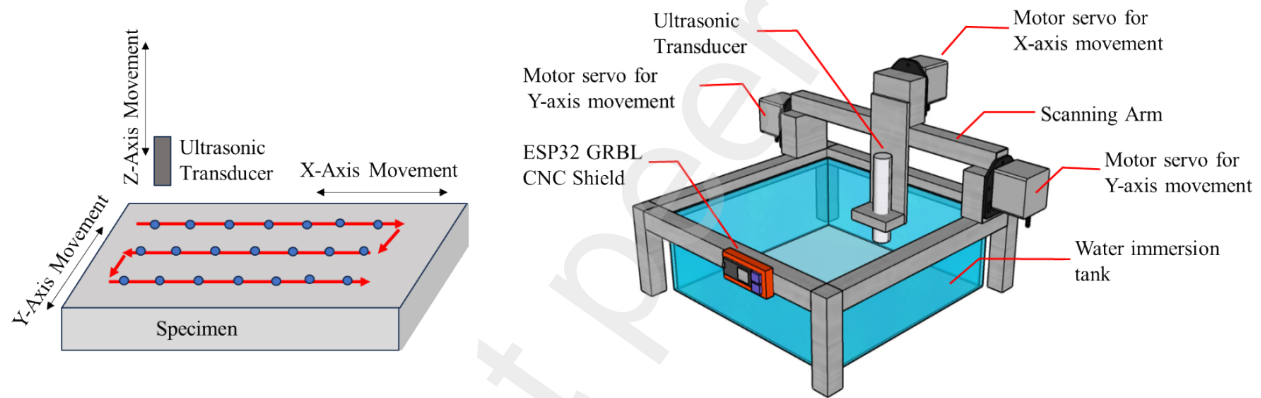


Figure 6. (a) A trajectory movement of the ultrasonic transducer and (b) The 3D design of the configurable scanning system

2.3. ULTRASONIC SIGNAL PROCESSING

An A-scan is the most basic form of representing ultrasonic testing results. In an A-scan, the signal generated by the ultrasonic transducer is plotted as a function of time, with the horizontal axis representing the time of data recording and the vertical axis representing the signal amplitude. From the A-scan, one can distinguish the ultrasonic echoes reflected from the upper and lower surfaces of the specimen as well as echoes caused by defects, allowing for defect identification. Nevertheless, in ultrasonic testing of thin laminated composite specimens, defects are still difficult to identify based on A-scan signals due to overlapping echoes, making it difficult to distinguish them. Therefore, the A-scan signals must be further processed using various data processing methods.

The processing of A-scan signals begins with filtering the A-scan signal using a bandpass filter. This filtering process removes noise that may arise from low or high frequencies. The frequency range of the filtered signal is determined based on the transducer's frequency. The next step is rectification, which involves converting negative data values to positive ones. The rectified signal is then processed further to create an envelope. The envelope creation process uses the A-scan signal's root mean square (RMS) method. The result of the envelope creation process for the A-scan signal measured in n point, the signal is defined as $A_n(t_i, x_i)$ where t_i is the i measurement time, with the increment of i adjusted to the data sampling rate, and x_i is the point location source of the A-scan signal.

By applying these data processing techniques, the ultrasonic testing system enhances the clarity and detectability of defects within the specimens. The filtered and enveloped A-scan signals provide a more precise

representation of the internal structure, facilitating accurate defect identification and characterization in thin laminated composite materials. The processing of the enveloped A-scan signal is illustrated in Figure 7.

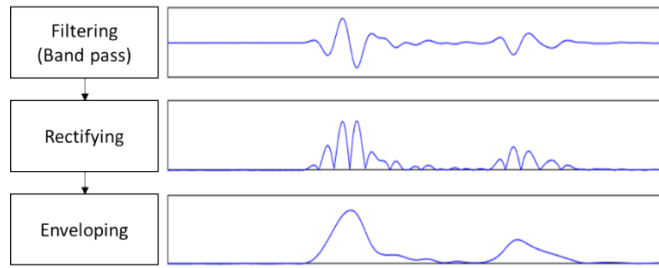


Figure 7. Enveloped A-scan signal processing

The defect identification process is carried out by comparing A_n at each measurement point with a reference signal. The reference signal is A_n at a point in the specimen that is known to be defect-free, thus characterizing a defect-free area. To increase the signal-to-noise ratio (SNR) of the reference signal is calculated by averaging several points of A_n as follows:

$$A_{ref} = \frac{1}{k} \sum_{k=1}^k (A_n) \quad (1)$$

where A_{ref} is the average value of the reference signal, and k is the number of data points used to calculate the reference value. This reference signal is only used for ultrasonic testing with the same specimen ultrasonic transducer and pulse ultrasonic setting.

The Pearson correlation equation is used to compare the measured signal at each point with the reference signal. This method was previously used for data processing in ultrasonic testing results [28]. Mathematically, the Pearson correlation equation is as follows:

$$r_n = \frac{\sum_{n=1}^n (A_n - \bar{A}_n)(A_{ref} - \bar{A}_{ref})}{\sqrt{\sum_{n=1}^n (A_n - \bar{A}_n)^2} \sqrt{\sum_{n=1}^n (A_{ref} - \bar{A}_{ref})^2}} \quad (2)$$

Where r_n is the correlation coefficient between the measurement signal at a point on the specimen and the reference signal, n is the number of measurement points, \bar{A}_n is the mean value of the measurement signal at a point on the specimen, and \bar{A}_{ref} is the mean value of the reference signal.

The value obtained from the Pearson correlation calculation ranges from 0 to 1. A value of 1 indicates a strong correlation between the reference signal and the measurement signal at a point on the specimen, suggesting that the point is defect-free. Conversely, a value of 0 indicates a weak correlation with the reference point, suggesting that the measured point is likely to have a defect. A threshold is necessary since the correlation values range from 0 to 1. This threshold can be determined using various methods. In this study, a statistical method is used to determine the threshold. Correlation values smaller than the threshold are identified as defect areas, while correlation values more significant than the threshold are identified as defect-free areas.

The collection of correlation values at all measurement points is then arranged into matrix V to be converted into a C-scan image based on the ultrasonic transducer's movement pattern, as shown in Figure 8. The value p changes according to the ultrasonic transducer's movement along the X-axis, while q changes according to its movement along the Y-axis. The matrix V is defined as follows:

$$V = \begin{pmatrix} r_{11} & \cdots & r_{p1} \\ \vdots & \ddots & \vdots \\ r_{1q} & \cdots & r_{pq} \end{pmatrix}, r_{pq} \in V, p = 1, 2, \dots; q = 1, 2, \dots \quad (3)$$

where q represents rows and p represents columns. The values of p and q are determined based on the direction and pattern of the scan during testing.

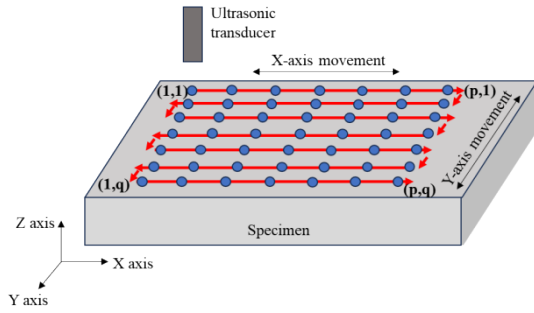


Figure 8. The typical scanning pattern

The reconstruction of the C-scan image is performed by displaying the matrix V in a heatmap format. Correlation values are displayed in a color gradient. This color gradient changes according to the determined threshold, which allows defects to be easily identified. Each correlation value in the matrix V represents one pixel in the generated C-scan image. The x and y axes on the heatmap correspond to the movement of the ultrasonic transducer along the X and Y orientations. The C-scan image reconstruction process is illustrated in Figure 9.

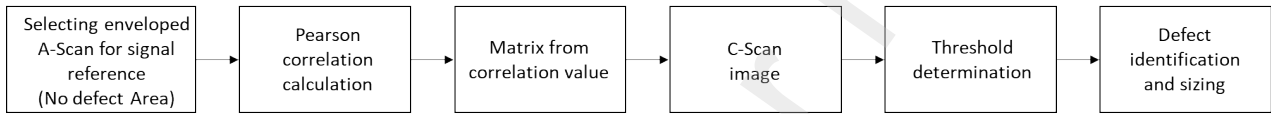


Figure 9. C-scan image reconstruction

3. EXPERIMENTAL SETUP

The testing was conducted to evaluate the performance of the developed ultrasonic NDT system. The testing setup began with preparing the equipment throughout the process. The configuration of the equipment used is illustrated in Figure 10. This set of equipment was placed on a table with a flat surface to ensure stability and consistency during testing. The table surface was flat to avoid influencing the ultrasonic wave measurement results.

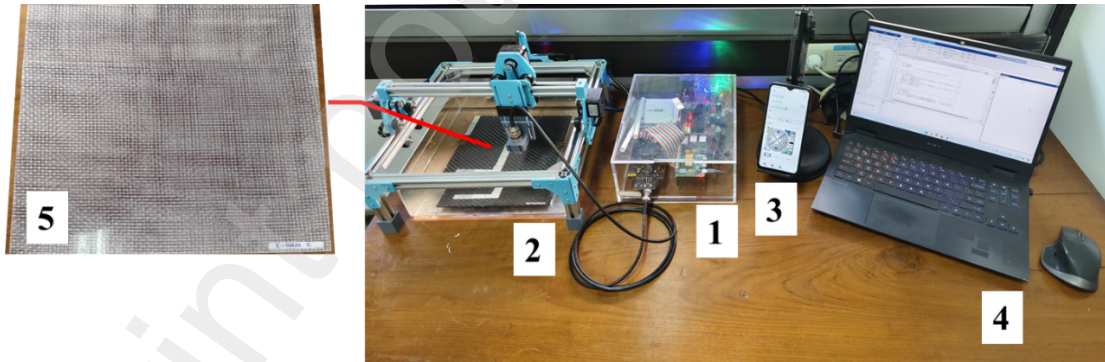


Figure 10. Experimental setup for specimen testing. (1). the pulser and ultrasonic measurement system, (2). the scanning system integrated with the water tank, (3). the smartphone containing the GUI for scanning system control, (4). the laptop used for data processing, and (5). the specimen to be tested.

The specimen was placed on a holder and secured with clamps inside the water tank. This positioning aimed to prevent direct adhesion of the specimen to the bottom of the water tank. This precaution is crucial because if the specimen adheres to the tank bottom, it would be challenging to distinguish ultrasonic echoes from the specimen from those reflected by the tank bottom surface. Both the specimen and the tank bottom surface had dimensions of 7 mm. Meanwhile, the transducer's position was adjusted to ensure a distance calculated based on the near field zone, dependent on the transducer's frequency and diameter. The experiment used an ultrasonic transducer with a probe diameter of 3/8 inch and frequency of 5 MHz. Figures 11-a and 11-b illustrate the specimen holder's position and the specimen's installation inside the water tank.

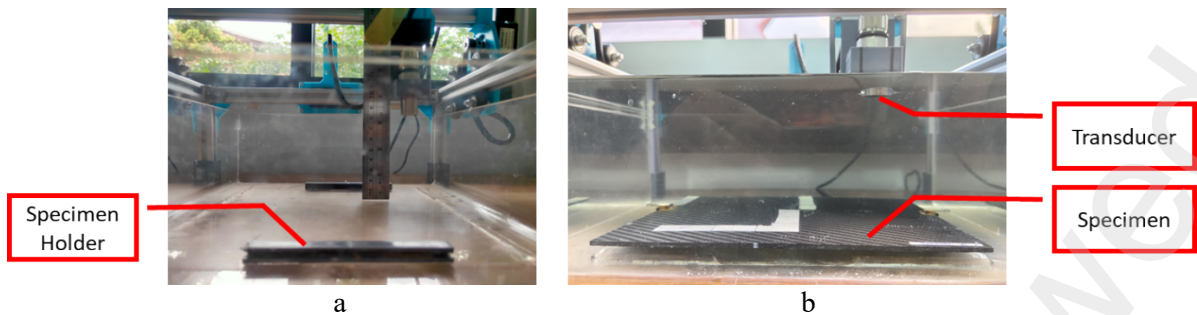


Figure 11. (a) specimen holder position, (b) specimen installation in the water tank

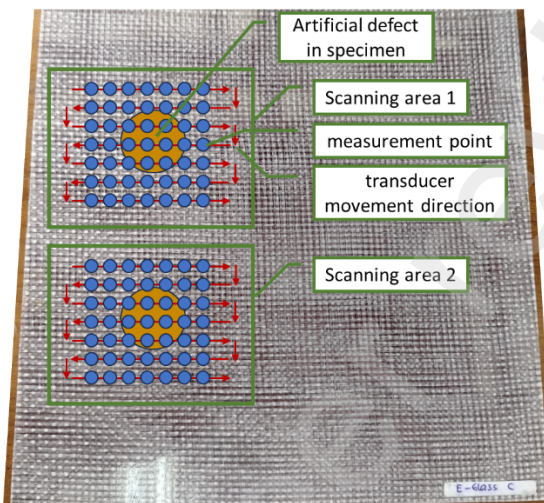


Figure 12. The scanning area location and transducer movement direction

The designed scanning system can perform a full surface scan of the fabricated specimen. However, for testing efficiency, the scanning process is focused on areas predicted to have defects according to the specimen's design. Therefore, this test includes two scanning areas. Scanning area 1 focuses on defects location 1 while scanning area 2 focuses on defects location 2. Each scanning area measures 70 mm x 70 mm. Each scanning area has ultrasonic transducer movement points along the X-axis and seven points along the Y-axis, with the transducer movement pattern following a raster pattern. Consequently, each scanning area comprises 49 measurement points with a spacing of 10 mm between each point. The scanning area position for each specimen, focusing on the artificial defect position, the direction of transducer movement, and the location and number of measurement points, is illustrated in Figure 12.

4. EXPERIMENTAL RESULTS

4.1. ULTRASONIC SIGNAL CHARACTERIZATION

The initial step in analyzing the ultrasonic testing results is to observe the characteristics of ultrasonic wave propagation in both specimens. The ultrasonic A-mode signals measured at locations predicted to be defect-free are processed using rectification and enveloping methods to facilitate the identification of ultrasonic wave reflections from the front wall echo (FWE) and back wall echo (BWE) of the material.

Figure 13 illustrates the processing of A-scan signals into rectified A-scan and enveloped A-scan for two types of composite materials, CFRP and GFRP. The graph's magenta line represents the rectified A-scan, and the dashed red line represents the enveloped A-scan for CFRP. The cyan line represents the rectified A-scan, and the dashed blue line represents the enveloped A-scan for GFRP. This graph shows that the FWE and BWE peaks can be identified in both composite materials. This analysis aids in understanding the wave propagation characteristics and assists in distinguishing between genuine material reflections and potential defects during ultrasonic testing of composite materials.

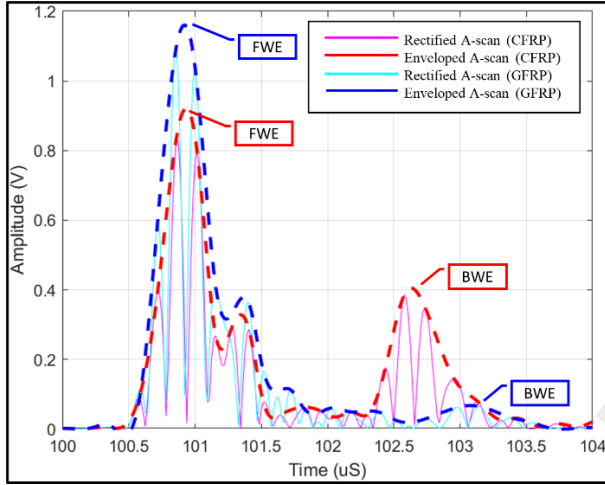


Figure 13. signal processing results in rectified and enveloped A-scan

The signal processing results indicate that the peak amplitude of the FWE for GFRP is higher than that for CFRP, with respective values of 1.161 volts and 0.922 volts. Conversely, the peak amplitude of the BWE for GFRP is lower than that for CFRP, being 0.075 volts compared to 0.405 volts. Based on these FWE and BWE amplitude values, the GFRP specimen demonstrates higher ultrasonic wave reflection characteristics than CFRP. It indicates that GFRP has higher reflection capability but lower penetration for ultrasonic waves emitted by the transducer.

The peak FWE amplitude for CFRP and GFRP occurs in about 100.938 μ s. However, the peak BWE amplitude for CFRP is 102.641 μ s, while for GFRP, it is at 103.109 μ s. Assuming a uniform thickness of 2.3 mm for both specimens, the ultrasonic wave propagation speed in CFRP is 2700.47 m/s, whereas in GFRP, it is 2118.95 m/s. It demonstrates that the ultrasonic wave propagation speed is higher in CFRP compared to GFRP.

4.2. ENVELOPED A-SCAN SIGNAL REFERENCE

In this study, the defect identification process utilized the Pearson correlation coefficient, which compares the measured A-scan envelope signal with a reference signal. Therefore, an accurate reference signal is required for each tested specimen condition.

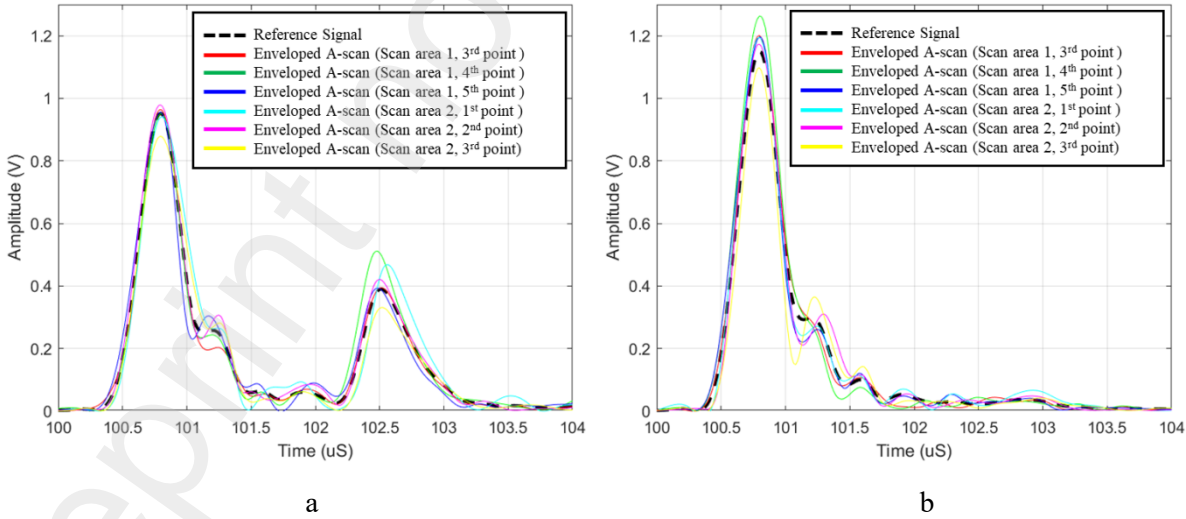


Figure 14. comparison of reference signal forms with enveloped a-scan signals measured at specific points
(a) in CFRP, (b) in GFRP

The reference signal was obtained by averaging the A-scan envelope signals at eight different points in the defect-free area of the specimen. Figure 14-a compares the reference and A-scan envelope signals at various locations on the CFRP specimen, representing a defect-free area. A black dashed line depicts the reference signal, while solid lines in various colors represent the A-scan envelope signals. For the GFRP specimen, the

comparison results are shown in Figure 14-b. Both graphs show that the reference signal is almost identical to the A-scan envelope signals in the defect-free areas.

4.3. DEFECT IDENTIFICATION BASED ON ENVELOPED A-SCAN

Figures 16 and 17 display enveloped A-scan graphs illustrating the ultrasonic echo response. These figures depict the differences in ultrasonic echo shapes between the reference signal (ultrasonic echo characteristics passing through defect-free areas) and the echoes passing through areas with defects locations 1 and 2. A dashed black line represents the reference signal, the blue line depicts the ultrasonic echo passing through the area with the defect location 1, and the red line shows the ultrasonic echo passing through the area with the defect location 2. An illustration of the transducer position and ultrasonic echo propagation during measurements on the specimen in defect-free areas, areas with defect locations 1, and areas with defect locations 2 is shown in Figure 15.

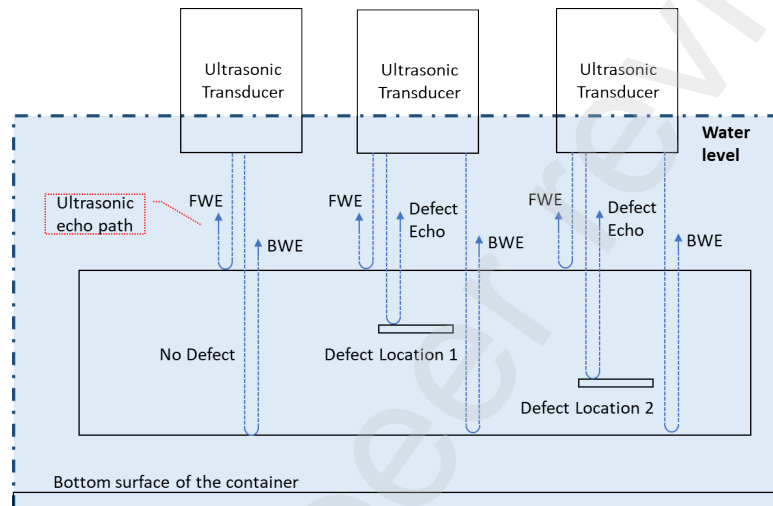


Figure 15. The differences in ultrasonic echo propagation from specimens during testing

Figure 16 shows the enveloped A-scan obtained from measurements performed on the CFRP specimen. It can be seen from the figure that the blue and red A-scan envelope signals exhibit new amplitude peaks, aside from the FWE and BWE peaks. These peaks are echoes caused by defects, referred to as defect echoes. The peak echoes for defect location 1 occur at $t = 101.234 \mu\text{s}$, while for defect location 2, they occur at $t = 101.938 \mu\text{s}$. The defect echo from location 1 appears earlier than location 2 because defect 1 is closer to the surface than defect 2. The presence of artificial defect inserts at locations 1 and 2 causes the BWE appearance to be delayed as the specimen thickness increases due to the addition of these inserts.

The peak defect echo due to the defect at location 1 is 0.764 volts, while the peak defect echo at location 2 is 0.377 volts. The difference in peak amplitude values of these echoes is due to the decreasing energy as the wave passes through deeper material. It indicates that ultrasonic waves experience higher attenuation when passing through deeper defects, resulting in lower peak amplitudes at deeper defect locations. Additionally, scattering occurring in the defect areas also contributes to the reduction in signal amplitude.

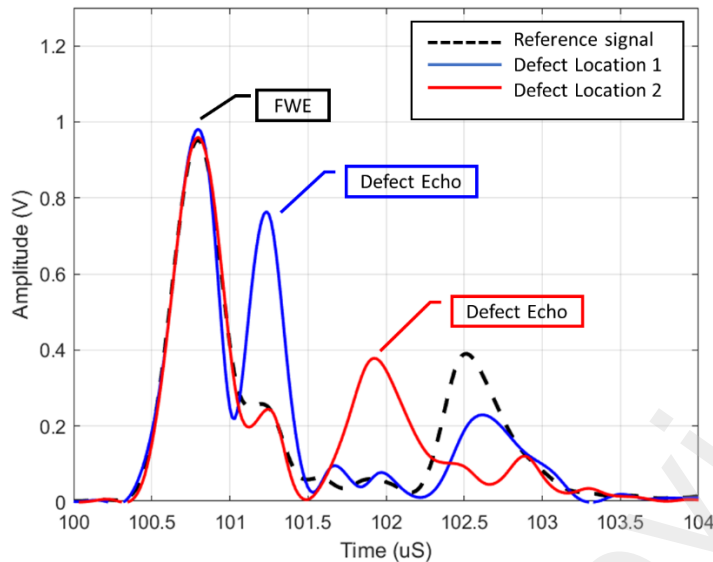


Figure 16. Enveloped A-scan in CFRP

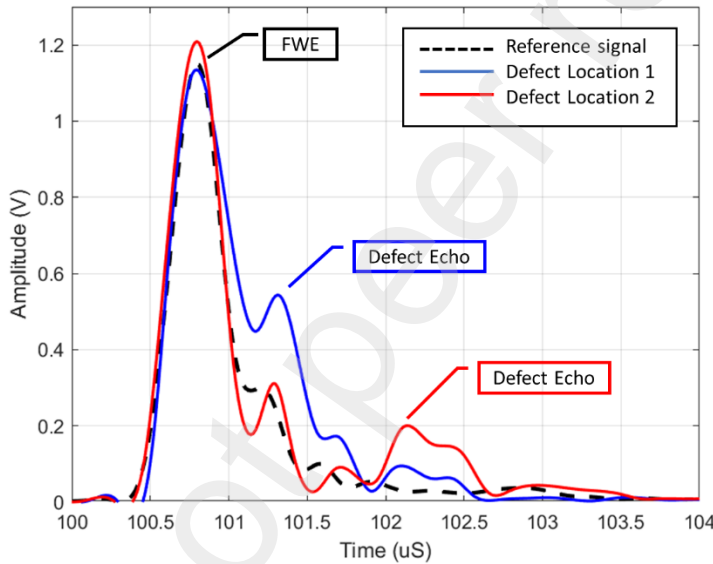


Figure 17. Enveloped A-scan in GFRP

Figure 17 shows the enveloped A-scan obtained from measurements performed on the GFRP specimen. From this figure, the appearance of defect echoes at both location 1 and location 2 can be observed, although the amplitudes of the defect echo at these locations differ. Based on Figures 16 and 17, it can be concluded that the developed ultrasonic NDT system can detect defects at various depths using the enveloped A-scan signals. It is demonstrated by the system's ability to identify defect echo peaks at different depths and show amplitude differences corresponding to the defect depths. This system effectively detects and characterizes defects in composite materials such as GFRP and CFRP.

4.4. SIGNAL CLASSIFICATION FOR NON-DEFECTIVE AND DEFECTIVE AREAS

The Pearson correlation coefficient is employed in ultrasonic NDT to classify defect and non-defect signals. This coefficient provides a statistical measure of the linear relationship between enveloped A-scan signals at each measurement point and reference signals, enabling the identification of defect and non-defect regions in composite materials. The calculated Pearson correlation coefficients from enveloped A-scan signals against reference signals are presented in Tables 1 and 2. Table 1 displays the Pearson correlation coefficients for CFRP specimens in scan area 1, while Table 2 shows the coefficients for GFRP specimens in the same area.

These tables are organized in a matrix format aligned with the position of the ultrasonic transducer during specimen testing, as depicted in Figure 8. Each table contains 49 values corresponding to the number of measurement points within a scan area. Here, the values of p and q range from 1 to 7, indicating positional changes along the X and Y axes within the scanning area. Further details on the placement of these values in the tables can be referenced in Figure 12.

Table 1 Pearson correlation coefficient in scanning area 1 of CFRP

Scanning Area 1 in CFRP							
\backslash q p	1	2	3	4	5	6	7
1	0.93	0.96	1.00	0.97	0.99	0.95	0.98
2	0.98	0.98	0.93	0.05	0.98	0.97	0.96
3	0.98	0.98	0.06	0.29	0.16	0.99	0.99
4	0.92	0.86	0.09	0.15	0.00	0.99	0.98
5	1.00	0.96	0.46	0.29	0.88	0.99	0.97
6	0.99	0.99	0.99	0.99	0.96	0.94	0.95
7	1.00	1.00	1.00	0.99	0.98	0.99	0.91

This table shows values outside the yellow-highlighted area range between 0.88 and 1.00, indicating defect-free areas. Conversely, the yellow-highlighted area shows Pearson correlation coefficient values ranging from 0 to 0.29, indicating the presence of defects. The table indicates that 8 points are showing the presence of defects.

Table 2. Pearson correlation coefficient in scanning area 1 of GFRP

Scanning Area 1 in GFRP							
\backslash q p	1	2	3	4	5	6	7
1	0.96	1.00	0.99	0.97	1.00	0.98	0.99
2	0.98	0.84	0.99	0.97	0.99	0.95	0.99
3	0.99	0.99	0.36	0.37	0.01	0.98	0.98
4	0.97	0.94	0.19	0.27	0.00	1.00	1.00
5	0.98	1.00	0.70	0.26	0.93	0.98	0.93
6	0.96	0.96	0.98	0.99	0.97	0.97	0.98
7	1.00	1.00	1.00	1.00	1.00	1.00	0.96

Furthermore, Table 2 shows that values not highlighted in yellow range from 0.84 to 1.00, indicating defect-free areas. In contrast, the yellow-highlighted area exhibits Pearson correlation coefficient values between 0 and 0.37, indicating the presence of defects. The table reveals that there are 7 points indicating the presence of defects. The consistency in value ranges between CFRP and GFRP specimens demonstrates the reliability of this method for detecting defects in various types of composite materials.

4.5. C-SCAN IMAGE RECONSTRUCTION

The results of ultrasonic NDT testing for both specimens using the developed system are represented in C-scans, as seen in Figures 18 and 19. The C-scan representation displays a heat map gradient with a jet color scheme. Defects are graphically represented using a color scale ranging from yellow to red, where the intensity reflects the severity of anomalies compared to the reference signal. Significant anomalies are shown in the red

region, while minor discrepancies are depicted in the brighter yellow region. Defect-free areas are depicted in blue; darker shades indicate higher similarity to the reference signal, indicating defect-free areas.

The C-scan images in Figures 18 and 19 are based on a matrix containing Pearson correlation coefficient values, consisting of 49 pixels arranged in a 7x7 matrix. This matrix is formed from seven measurement points along the X-axis and seven points along the Y-axis, with a measurement point spacing of 10 mm. Through linear interpolation, each pixel in the image represents a distance of 1 mm, creating a smoother visualization without square artifacts.

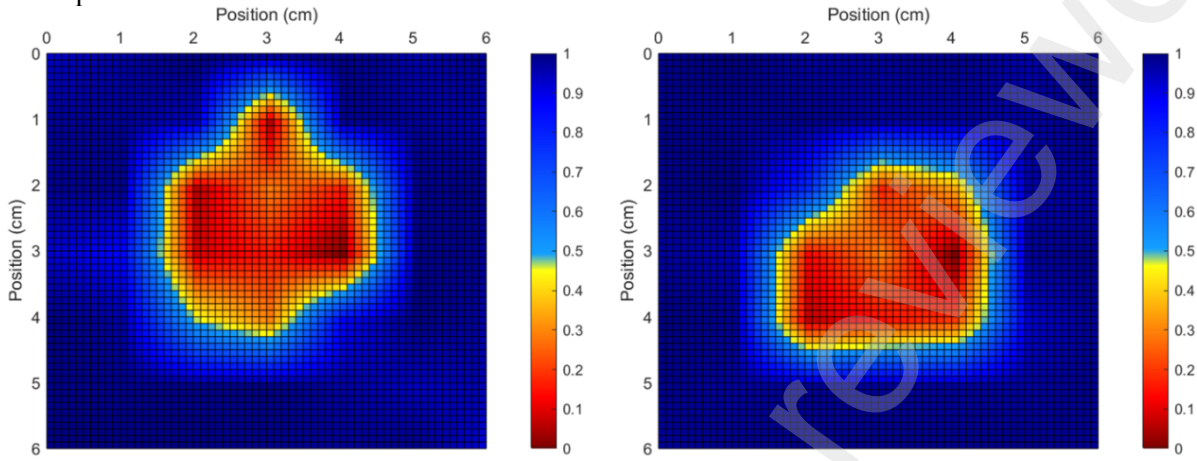


Figure 18. C-scan images of CFRP with artificial defect in (a) location one, (a) and (b) location two

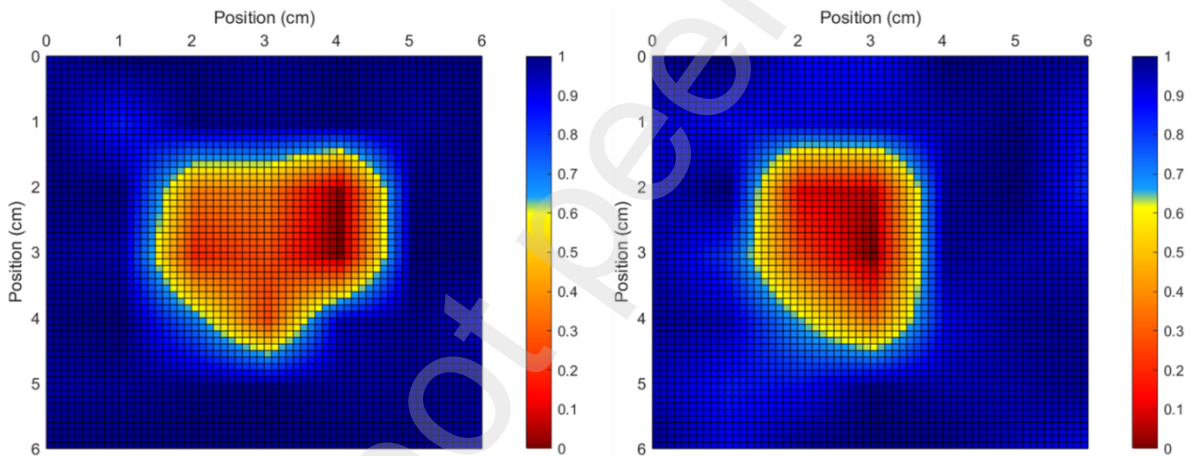


Figure 19. C-scan images of GFRP with an artificial defect in (a) location one (a) and (b) location two

Based on Figures 18 and 19, defects are observed in both CFRP and GFRP specimens at locations 1 and 2. These defects appear smaller at location 2 compared to location 1 in both specimens. It indicates that the depth of defects influences the ultrasonic NDT testing results. This influence is evident in the enveloped A-scan signal graphs in Figures 16 and 17, where the peak amplitudes of defect echoes weaken with increased depth, particularly in GFRP material. However, from these four figures, it can be concluded that the developed system effectively produces C-scan images for both types of materials, CFRP and GFRP, with variations in defect depth.

4.6. ESTIMATION OF ARTIFICIAL DEFECT AREA

A methodology to calculate the size of defect areas is essential for determining their dimensions. A straightforward approach involves counting the number of pixels identified as defect areas. Each pixel value in the C-scan image represents a Pearson correlation coefficient. A pixel is categorized as a defect area if its Pearson correlation coefficient falls below a predefined threshold. This study's threshold method is based on mean and standard deviation. The calculated defect area sizes are then compared with the actual sizes of artificial defects to assess percentage errors, serving as a metric to evaluate the performance of the proposed system development. Measurements of defects and corresponding percentage errors for both specimens are presented in Table 3.

Table 3. Comparison of actual and measured defect area sizes.

Type of Specimen	Area (mm ²)	% Error
Artificial defect (circle with r = 15mm)	707	-
CFRP with a defect in location 1	706	0,14
CFRP with a defect in location 2	673	4,81
GFRP with a defect in location 1	705	0,28
GFRP with a defect in location 2	576	18,53

Table 3 illustrates how the depth position of defects influences defect measurement results. Specifically, defects at location 1 in the CFRP specimen have an error rate of 0.14%, while in the GFRP specimen, it is 0.28%. These values are significantly lower than the error rates for defects at location 2, which are 4.81% in the CFRP specimen and 18.53% in the GFRP specimen. Using the same approach, the CFRP specimen shows a lower error rate than the GFRP specimen.

5. DISCUSSIONS

This discussion focuses on comparing the performance of the developed ultrasonic NDT system in this study with commercial ultrasonic NDT equipment used in previous research. For instance, Hasiotis et al. traced defects in laminate composite materials using ultrasonic methods [29]. Papa et al. inspected composites to detect impact-induced defects [30]. Additionally, Ciecieląg et al. utilized ultrasonic C-scan to analyze actual defects in composite materials [31].

Similar to findings from previous studies using commercial ultrasonic NDT systems, this research's developed ultrasonic NDT system successfully depicts differences in ultrasonic wave propagation characteristics within CFRP and GFRP materials. The system also identifies simulated inclusion defects in the form of circular artificial defects with a radius of 15 mm placed at Location 1 (between the third and fourth fiber layers) and Location 2 (between the seventh and eighth fiber layers) by analyzing the generated enveloped A-scan signals. Moreover, the system accurately predicts and displays defect sizes in C-scan images. The predicted defect size error at Location 1 shows 0.14% for CFRP and 0.28% for GFRP specimens.

However, when identifying artificial defects at Location 2, the predicted defect sizes still exhibit significant errors, namely 4.81% for CFRP and 18.53% for GFRP specimens. It is due to the attenuation of ultrasonic echo energy with increasing material depth, which affects the identification of deeper defects, as observed in Figures 15 and 16. Further development is needed to address this, such as adding hardware or implementing Time Gain Compensation (TGC) algorithms to enhance signals weakened by material depth effects.

Overall, the defect identification process using the developed system at locations 1 and 2 yielded measurement results with lower percentage errors in the CFRP specimens. This outcome underscores the system's effectiveness in accurately detecting and measuring defects in CFRP materials. In contrast, measurements on the GFRP specimens exhibited higher errors than those of CFRP. This discrepancy can be attributed to GFRP's unique properties, such as its higher reflection capability and lower penetration for ultrasonic waves emitted by the transducer [32]. These characteristics of GFRP, as illustrated in Figure 13, influence the accuracy of defect detection, highlighting the challenges and nuances in applying ultrasonic NDT techniques across different composite materials.

Commercial ultrasonic NDT equipment available on the market outperforms the Programmable Portable Ultrasonic NDT System proposed here regarding accuracy and other technical aspects. Nonetheless, The Programmable Portable Ultrasonic NDT System possesses several significant advantages. Its open-source device design and concept help minimize manufacturing costs, whereas commercial ultrasonic NDT equipment tends to be relatively expensive. This system also accesses raw data, is compatible with different sensors and specimens, and can be reconfigured by integrating different signal processing algorithms to enhance data accuracy and processing efficiency. Furthermore, equipped with wireless communication capabilities, it enables remote access, enhancing portability and flexibility across various environmental conditions.

Considering these reasons, the proposed Programmable Portable Ultrasonic NDT System is suitable and capable of use in laboratory-scale quality control activities for laminated composite production outcomes. It is well-suited to support research activities in research institution laboratories and can be employed by small—to medium-sized industries involved in UAV composite fabrication.

6. CONCLUSIONS

The developed portable programmable ultrasonic NDT system, utilizing open-source hardware, effectively identifies simulated inclusion defects in CFRP and GFRP laminated composite materials commonly used in UAV structural manufacturing. Performance testing of the system demonstrates accurate results, affirming its reliability. It enables detailed analysis of material characteristics by presenting ultrasonic test results in both A-scan and C-scan representations.

Furthermore, its advantages include the flexibility to be reprogrammed according to testing needs and cost-effectiveness compared to commercial ultrasonic NDT equipment. These features make the system suitable for ensuring quality control in producing laminated composite materials, both in laboratory-scale settings and by small—to medium-sized industries involved in UAV manufacturing. Thus, it ensures the quality of the composite materials produced.

Acknowledgments

- The authors thank Institut Teknologi Bandung, Indonesia, for supporting this research.
- The author would like to thank the Indonesia Endowment Fund for Education Agency (LPDP) of the Republic of Indonesia for financial support for the author's magister study.

References

- [1] M. M. ElFaham, A. M. Mostafa, and G. M. Nasr, "Unmanned aerial vehicle (UAV) manufacturing materials: Synthesis, spectroscopic characterization and dynamic mechanical analysis (DMA)," *J Mol Struct*, vol. 1201, p. 127211, Feb. 2020, doi: 10.1016/j.molstruc.2019.127211.
- [2] M. S. H. Al-Furjan, L. Shan, X. Shen, M. S. Zarei, M. H. Hajmohammad, and R. Kolahchi, "A review on fabrication techniques and tensile properties of glass, carbon, and Kevlar fiber reinforced polymer composites," *Journal of Materials Research and Technology*, vol. 19, pp. 2930–2959, Jul. 2022, doi: 10.1016/j.jmrt.2022.06.008.
- [3] T. Ramakrishnan *et al.*, "Study of Numerous Resins Used in Polymer Matrix Composite Materials," *Advances in Materials Science and Engineering*, vol. 2022, pp. 1–8, Mar. 2022, doi: 10.1155/2022/1088926.
- [4] K. Abdurohman, T. Satrio, N. L. Muzayadah, and Teten, "A comparison process between hand lay-up, vacuum infusion and vacuum bagging method toward e-glass EW 185/lycal composites," *J Phys Conf Ser*, vol. 1130, no. 1, p. 012018, Nov. 2018, doi: 10.1088/1742-6596/1130/1/012018.
- [5] F. SHAIK, M. RAMAKRISHNA, and P. D. VARMA, "A Review on Fabrication of Thermoset Prepreg Composites using Out-of-Autoclave Technology," *INCAS BULLETIN*, vol. 13, no. 2, pp. 133–149, Jun. 2021, doi: 10.13111/2066-8201.2021.13.2.13.
- [6] D. K. Rajak, P. H. Wagh, and E. Linul, "Manufacturing Technologies of Carbon/Glass Fiber-Reinforced Polymer Composites and Their Properties: A Review," *Polymers (Basel)*, vol. 13, no. 21, p. 3721, Oct. 2021, doi: 10.3390/polym13213721.
- [7] M. J. Suriani, H. Z. Rapi, R. A. Ilyas, M. Petru, and S. M. Sapuan, "Delamination and Manufacturing Defects in Natural Fiber-Reinforced Hybrid Composite: A Review," *Polymers (Basel)*, vol. 13, no. 8, p. 1323, Apr. 2021, doi: 10.3390/polym13081323.
- [8] J. Chen, Z. Yu, and H. Jin, "Non-destructive testing and evaluation techniques of defects in fiber-reinforced polymer composites: A review," *Front Mater*, vol. 9, Oct. 2022, doi: 10.3389/fmats.2022.986645.
- [9] B. Wang, S. Zhong, T. L. Lee, K. S. Fancey, and J. Mi, "Non-destructive testing and evaluation of composite materials/structures: A state-of-the-art review," *Advances in Mechanical Engineering*, vol. 12, no. 4. 2020. doi: 10.1177/1687814020913761.
- [10] W. Harizi, S. Chaki, G. Bourse, and M. Ourak, "Mechanical damage characterization of glass fiber-reinforced polymer laminates by ultrasonic maps," *Compos B Eng*, vol. 70, pp. 131–137, Mar. 2015, doi: 10.1016/j.compositesb.2014.11.014.
- [11] K. Yadav, R. Kumar, N. Dhiman, S. Yadav, and P. K. Dubey, "Development and study of ultrasonic immersion testing system for industrial and metrological application," *Journal of Instrumentation*, vol. 18, no. 03, p. P03001, Mar. 2023, doi: 10.1088/1748-0221/18/03/P03001.

- [12] N. J. Blackman, D. A. Jack, and B. M. Blandford, "Improvement in the Quantification of Foreign Object Defects in Carbon Fiber Laminates Using Immersion Pulse-Echo Ultrasound," *Materials*, vol. 14, no. 11, p. 2919, May 2021, doi: 10.3390/ma14112919.
- [13] M. Ma *et al.*, "High Precision Detection Method for Delamination Defects in Carbon Fiber Composite Laminates Based on Ultrasonic Technique and Signal Correlation Algorithm," *Materials*, vol. 13, no. 17, p. 3840, Aug. 2020, doi: 10.3390/ma13173840.
- [14] M. Slamani and J.-F. Chatelain, "A review on the machining of polymer composites reinforced with carbon (CFRP), glass (GFRP), and natural fibers (NFRP)," *Discover Mechanical Engineering*, vol. 2, no. 1, p. 4, Apr. 2023, doi: 10.1007/s44245-023-00011-w.
- [15] S. Hegde, B. Satish Shenoy, and K. N. Chethan, "Review on carbon fiber reinforced polymer (CFRP) and their mechanical performance," *Mater Today Proc*, vol. 19, pp. 658–662, 2019, doi: 10.1016/j.matpr.2019.07.749.
- [16] P. Morampudi, K. K. Namala, Y. K. Gajjela, M. Barath, and G. Prudhvi, "Review on glass fiber reinforced polymer composites," *Mater Today Proc*, vol. 43, pp. 314–319, 2021, doi: 10.1016/j.matpr.2020.11.669.
- [17] Y.-C. Liang, P.-C. Chin, Y.-P. Sun, and M.-R. Wang, "Design and Manufacture of Composite Landing Gear for a Light Unmanned Aerial Vehicle," *Applied Sciences*, vol. 11, no. 2, p. 509, Jan. 2021, doi: 10.3390/app11020509.
- [18] W. S. Chin and D. G. Lee, "Laminating rule for predicting the dielectric properties of E-glass/epoxy laminate composite," *Compos Struct*, vol. 77, no. 3, pp. 373–382, Feb. 2007, doi: 10.1016/j.compstruct.2005.07.019.
- [19] M. Hafid, A. Nurrohmadi, and R. A. Ramadhan, "NUMERICAL INVESTIGATION ON THE FUSELAGE AIRFRAME OF LSU 05 NG AIRCRAFT," *Jurnal Teknologi Dirgantara*, vol. 18, no. 2, p. 93, Dec. 2020, doi: 10.30536/j.jtd.2020.v18.a3327.
- [20] A. Zarei, S. Farahani, and S. Pilla, "An experimental study on the manufacturing of engineered defects in composite plates," *Composites Part C: Open Access*, vol. 9, p. 100327, Oct. 2022, doi: 10.1016/j.jcomc.2022.100327.
- [21] M. Barzegar, D. J. Pasadas, A. L. Ribeiro, and H. G. Ramos, "Comparative Study on Ultrasonic C-Scan Imaging of Composite Lap Joints Using Piezoelectric Transducer: Pulse-Echo and Pitch-Catch Configurations," *IEEE Trans Instrum Meas*, vol. 73, pp. 1–10, 2024, doi: 10.1109/TIM.2024.3368490.
- [22] L. Jonveaux, "un0rick: open-source fpga board for single element ultrasound imaging", doi: 10.5281/zenodo.3364559.
- [23] H. Susanti, H. Mukhtar, S. Suprijanto, and W. A. Cahyadi, "Initial Study of A-mode Ultrasound Spectroscopy Through Mechanical Wave Scattering Phenomenon for Measuring 3D-printed Bone Model Density," *International Journal of Mechanics*, vol. 17, pp. 74–79, Aug. 2023, doi: 10.46300/9104.2023.17.11.
- [24] A. P. Hariyanto, N. T. Budiarti, Suprijanto, K. H. Ng, F. Haryanto, and Endarko, "Evaluation of physical properties and image of polyvinyl chloride as breast tissue equivalence for dual-modality (mammography and ultrasound)," *Phys Eng Sci Med*, vol. 46, no. 3, pp. 1175–1185, Sep. 2023, doi: 10.1007/s13246-023-01283-y.
- [25] Luc Jonveaux, "Open-source ultrasound." Accessed: Jul. 10, 2024. [Online]. Available: <http://un0rick.cc/>
- [26] Bdring, "Grbl (CNC Controller) For ESP32." Accessed: Jul. 10, 2024. [Online]. Available: https://github.com/bdring/Grbl_Esp32
- [27] Luc, "ESP3D-WEBUI." Accessed: Jul. 10, 2024. [Online]. Available: <https://github.com/luc-github/ESP3D-WEBUI>
- [28] Y. Chang, D. Yang, and Y. Guo, "Laser ultrasonic damage detection in coating-substrate structure via Pearson correlation coefficient," *Surf Coat Technol*, vol. 353, pp. 339–345, Nov. 2018, doi: 10.1016/j.surfcoat.2018.09.005.
- [29] T. Hasiotis, E. Badogiannis, and N. G. Tsouvalis, "Application of Ultrasonic C-Scan Techniques for Tracing Defects in Laminated Composite Materials," *Strojniški vestnik – Journal of Mechanical Engineering*, vol. 2011, no. 03, pp. 192–203, Mar. 2011, doi: 10.5545/sv-jme.2010.170.

- [30] I. Papa, V. Lopresto, and A. Langella, "Ultrasonic inspection of composites materials: Application to detect impact damage," *International Journal of Lightweight Materials and Manufacture*, vol. 4, no. 1, pp. 37–42, Mar. 2021, doi: 10.1016/j.ijlmm.2020.04.002.
- [31] K. Ciecieląg, K. Kęcik, A. Skoczylas, J. Matuszak, I. Korzec, and R. Zaleski, "Non-Destructive Detection of Real Defects in Polymer Composites by Ultrasonic Testing and Recurrence Analysis," *Materials*, vol. 15, no. 20, p. 7335, Oct. 2022, doi: 10.3390/ma15207335.
- [32] M. E. Ibrahim, "Ultrasonic inspection of hybrid polymer matrix composites," *Compos Sci Technol*, vol. 208, p. 108755, May 2021, doi: 10.1016/j.compscitech.2021.108755.